Sensitive detection of endocrine disrupters using ionic liquid – Single walled carbon nanotubes modified screen-printed based biosensors

Ana-Maria Gurban[a], Lucian Rotariu[a,b], Mihaela Baibarac[c], Ioan Baltog[c], Camelia Bala[a,b,*]

[a] Laboratory of Quality Control and Process Monitoring, University of Bucharest, 4-12 Regina Elisabeta, 030018 Bucharest, Romania
[b] Department of Analytical Chemistry, University of Bucharest, 4-12 Regina Elisabeta, 030018 Bucharest, Romania
[c] Laboratory of Optical Process in Nanostructured Materials, National Institute of Materials Physics, P.O. Box MG-7, Bucharest R077125, Romania

ARTICLE INFO

ABSTRACT

Simple and low cost biosensor based on screen-printed electrode for sensitive detection of some alkylphenols was developed, by entrapment of HRP in a nanocomposite gel based on single-walled carbon nanotubes (SWCNTs) and 1-butyl-3-methylimidazolium hexafluorophosphate ([BMIM][PF_6]) ionic liquid. Raman and FTIR spectroscopy, CV and EIS studies demonstrate the interaction between SWCNTs and ionic liquid. The nanocomposite gel, SWCNT–[BMIM][PF_6] provides to the modified sensor a considerable enhanced electrocatalytic activity toward hydrogen peroxide reduction. The HRP based biosensor exhibits high sensitivity and good stability, allowing a detection of the alkylphenols at an applied potential of −0.2 V vs. Ag/AgCl, in linear range from 5.5 to 97.7 μM for 4-t-octylphenol and respectively, between 5.5 and 140 μM for 4-n-nonylphenol, with a response time of about 5 s. The detection limit was 1.1 μM for 4-t-octylphenol, and respectively 0.4 μM for 4-n-nonylphenol (S/N = 3).

© 2011 Elsevier B.V. All rights reserved.

1. Introduction

The endocrine disrupting chemicals (EDCs), a class of substances defined not by chemical nature but by biological effect, affecting the population health have attracted great interest [1,2]. They include pesticides, polycyclic aromatic hydrocarbons (PAHs), phthalate plasticizers, alkylphenols (APs), bisphenol A, polychlorinated biphenyls (PCBs), dioxins, surfactants, synthetic steroids, brominated flame retardants, parabens and are potentially present in food as phytoestrogens. From all these, nonylphenol has been designated as a member of the endocrine disrupters, more specifically, pseudoestrogens, which are suggested to be related to the decline of human and wildlife reproductive health. Octylphenol is very toxic to aquatic organisms, is not easily degraded in the environment and has the potential to cause significant endocrine disruption effects.

Some analytical techniques reported for EDCs detection are fluorescence immunoassays which are able to detect endocrine disrupting compounds in wastewater [3], liquid chromatography coupled with mass spectrometer (LC–MS) and ELISA technique which provide detection of the most important classes of EDCs in food and environment at levels of biological significance [4].

The levels of concentrations of EDCs in different sample are low (1–72,000 ng L^{-1}) and due to the complexity of the environmental matrices, pre-concentration of the samples is required before LC–MS analysis [5,6].

All the reported techniques are reaching the highest accuracy with low detection limits, but are expensive, time-consuming, and require the use of highly trained personnel. The development of biosensors as analytical devices for fast, low cost, reliable and sensitive determinations is a result of the current demand for field monitoring. These devices can be used both by regulatory authorities and by industry to provide enough information for routine testing and screening of samples [7].

Yin et al. [8] have developed an amperometric sensor based on CoTe quantum dots and poly (amidoamine) dendrimers (PAMAM) immobilized onto glassy carbon electrode using layer-by-layer assembly technique for determination of trace amounts of bisphenol A. Nonylphenol was determined by Evtugyn et al. [9], using an immunosensor obtained by immobilisation of specific antibodies together with horseradish peroxidase (HRP) on the surface of carbon screen-printed electrodes. The detection limit achieved was 10 μg L^{-1} for nonylphenol. A human recombinant estrogen receptor was used in the competitive assay mode by Usami and Ohno [10] for detection of 4-nonylphenol. Indirect ELISA and fluorescence polarization immunoassay protocols have been used for detection of 1 mg L^{-1} nonylphenol by Yakovleva et al. [11]. Detection of 10–100 μg L^{-1} 4-n-nonylphenol was achieved by competitive immunoassays in the format of microtitre
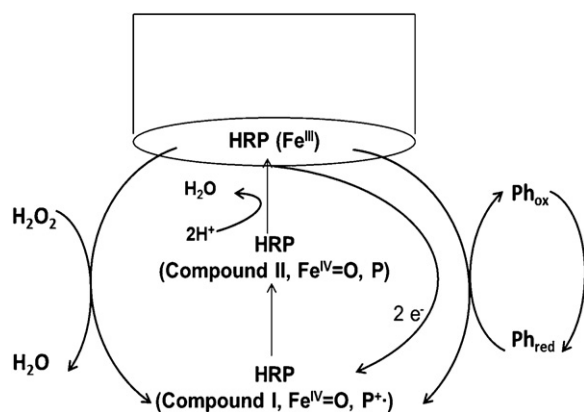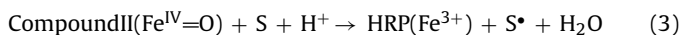
Fig. 1. Detection of phenolic compound using a HRP based biosensor.

plate ELISA and dipstick tests involving monoclonal antibodies [12].

Biosensors based on tyrosinase were also reported in literature for the detection of phenols [13,14]. The main drawbacks of these biosensors include the electrode fouling due to a radical polymerisation and the deactivation of enzyme by o-quinone generated in the enzymatic reaction. Other reported biosensors for the detection of phenolic compounds use laccase to catalyze the oxidation of analyte. Many of these are based on oxygen consumption that is not very convenient from analytical point of view. Systems using both laccase and tyrosinase have been reported as well [15].

HRP based biosensors represent an alternative to the above systems. HRP is a very stable and active enzyme as it was previously demonstrated after immobilization on the surface of SWCNT-Prussian blue modified screen-printed electrode [16]. The general principle for detection of phenolic compounds using biosensors based on horseradish peroxidase is presented in Fig. 1. HRP catalyzes the oxidation of electron donor substrates (e.g. phenols, amines, aminophenols, etc.) with hydrogen peroxide in three steps, as following [17,18].

$$HRP(Fe^{3+}) + H_2O_2 \rightarrow CompoundI + H_2O \tag{1}$$

$$CompoundI(Fe^{IV}\!-\!O, P^{+\bullet}) + S + H^+ \rightarrow CompoundII(Fe^{IV}\!-\!O) + S^\bullet \tag{2}$$

$$CompoundII(Fe^{IV}\!=\!O) + S + H^+ \rightarrow HRP(Fe^{3+}) + S^\bullet + H_2O \tag{3}$$

The H_2O_2 is reduced in a first step and an oxidized enzyme intermediate, called Compound I, is formed (reaction (1)). Compound I consisting in an oxyferryl iron ($Fe^{IV}\!=\!O$) and a radical, a porphyrin π–cation radical, is reduced in two steps, when a donor substrate (S) is oxidized to a radical product ($S^\bullet$) (reactions (2) and (3)). The formed radicals ($S^\bullet$) are reduced by the electrode, at an applied potential vs. Ag/AgCl, the current reduction being proportional with the substrate concentration (reaction (4)) [18].

$$S^\bullet + e^- + H^+ \rightarrow S \tag{4}$$

In the last years, a series of biosensors based on carbon nanotubes modified electrodes or different composites based on ionic liquids has been reported for H_2O_2 detection, but none was used further for alkylphenols detection. The high stability, high electrical conductivity and very low vapour pressure, make ionic liquids versatile and promising for electrochemistry of enzymes and a suitable media for supporting biocatalytic processes [19,20].

Chen et al. [21] have used Nafion as binder to form Nafion-ionic liquids composite film, helping [BMIM][PF_6] to adhere on the glassy carbon electrode, and using further this composite film as immobilisation matrix to entrap HRP. Fan et al. [22] developed an electrochemical biosensor for direct electrochemistry of HRP, using a glassy carbon electrode modified with Nafion, agarose hydrogel

and [BMIM][PF_6] ionic liquid composite as sensing platform. This biosensor detected the H_2O_2 with a detection limit of 0.12 μM. A third generation biosensor for hydrogen peroxide was constructed by Xu et al. [23] through crosslinking horseradish peroxidase (HRP) onto a glassy carbon electrode modified with multiwall carbon nanotubes (MWNTs). Glutaraldehyde and bovine serum albumin were used to cross-link HRP and the MWNTs, and the detection limit achieved with this biosensor was 0.4 μM H_2O_2.

Others have used nonenzymatic systems for electrocatalytic reduction of hydrogen peroxide (H_2O_2) [24,25]. Li et al. [25] electro-polymerized Prussian blue (PB) on a carbon ionic liquid electrode (CILE), while Wang et al. [24] electro-polymerized aniline and single-walled carbon nanotubes on a platinum electrode in a room temperature ionic-liquid.

Our work has been focused on development of an amperometric biosensor based on screen-printed electrodes modified with a nanocomposite film, consisting in SWCT-[BMIM][PF_6] and HRP, for sensitive detection of 4 n-nonylphenol and 4-t-octylphenol. This biosensor combines the advantages of both ionic liquids and CNTs.

The modified screen-printed electrodes were characterized by cyclic voltammetry (CV), amperometry and electrochemical impedance spectroscopy (EIS). The nanocomposite film facilitates the electrochemistry of HRP and the reduction of hydrogen peroxide (H_2O_2), allowing further the sensitive detection of endocrine disrupters, 4-n-nonylphenol and respectively, 4-t-octylphenol.

2. Experimental

2.1. Chemicals and reagents

Single-walled carbon nanotube (0.5–100 μm length, 1.1 nm diam.), N,N-dimethylformamide (DMF) (99%), horseradish peroxidase 25 kU (E.C.1.11.1.7, RZN3), 1-butyl-3-methylimidazolium hexafluorophosphate, potassium hexacyanoferrate (III), potassium hexacyanoferrate (II), tetramethoxysilane (TMOS), polyethyleneglycol (PEG600), 4-t-octylphenol (97%) were supplied from Sigma–Aldrich. The Nafion (perfluorinated ion-exchange resin, 5% solution in a mixture of lower aliphatic alcohols and water), hydrogen peroxide solution (30%), acetonitrile (>99.9%, GC) and methyltrimethoxysilane (MTMOS) were provided by Fluka, while the phenol (97%), HCl 37% and 4-n-nonylphenol (99.9%) were provided by Riedel-de Haën. All other chemicals were of analytical grade.

All aqueous solutions were prepared with ultrapure water, obtained with a Millipore system (18.2 MΩ cm). A 0.05 M phosphate buffer solution (PBS, pH 7.4) containing 0.1 M KCl was used as supporting electrolyte. The pH 7.4 of buffer solution has been optimized for HRP in our previous work [16]. A fresh stock solution of 20 mM H_2O_2 was prepared daily. Standard solutions of 5 mM alkylphenols were prepared in acetonitrile.

2.2. Apparatus and measurements

Electrochemical measurements were carried out using a BAS 100B Electrochemical Workstation (BAS, West Lafayette, USA) in a conventional three-electrode electrochemical cell of 5 mL. All the experiments were carried out at room temperature, using a system of screen-printed electrodes (SPE) Dropsens – DRP110. The working (4 mm diameter) and the counter electrodes are made of carbon and the reference electrode is made of Ag. Cyclic voltammetry experiments have been performed in the potential range of −0.6 to 1 V, with a scan rate of $0.1\,V\,s^{-1}$. Amperometric measurements were carried out under constant stirring (500 rpm). All potentials are referred to Ag pseudo-reference electrode. Electrochemical impedance spectroscopy (EIS) measurements were performed with
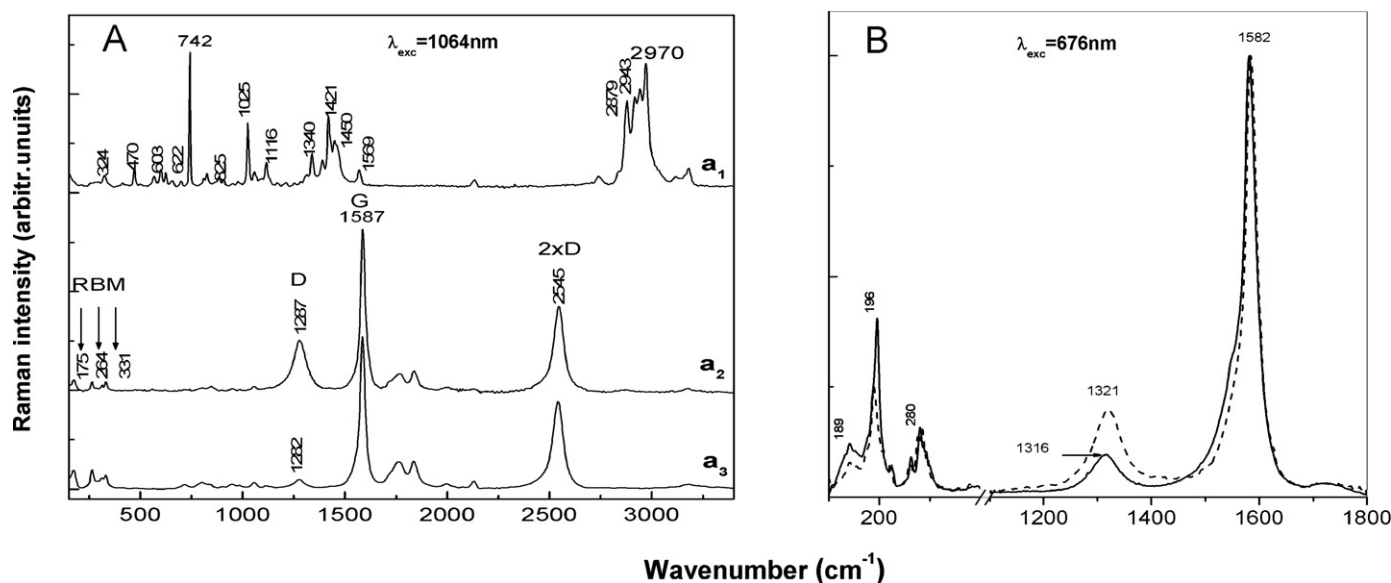
Fig. 2. (A) Raman spectra recorded at 1064 nm excitation wavelength of [BMIM][PF$_6$] (a$_1$), SWNTs (a$_2$) and the SWNT-[BMIM][PF$_6$] gel (a$_3$). (B) Raman spectra recorded at 676 nm excitation wavelength of SWNTs (solid line) and the SWNTs/[BMIM][PF$_6$] mixture (dashed line).

an Autolab PGSTAT 12 (Eco Chemie, Ultrecht, Netherlands) electrochemical system. A Bandelin Sonorex RK156 ultrasonic bath was used for preparation of the SWCNT–[BMIM][PF$_6$] nanocomposite gel.

Raman spectra were recorded at room temperature and in backscattering geometry under 676 and 1064 nm excitation wavelengths, using Jobin Yvon T64000 and FT Raman Bruker RFS 100 spectrophotometers, respectively.

FTIR spectra were recorded using a Tensor 27 FT-IR spectrometer, equipped with Hyperion 3000 FT-IR microscope endowed with a Grazing Angle Objective. All Raman and FTIR spectra of analyzed compounds in this paper were deposited on Au supports prepared by vacuum evaporation technique.

2.3. Preparation of nanocomposite modified sensors

CNTs can be solubilized in ionic liquids (ILs) due to cation–π interactions, CNTs enhancing the conductivity of the system [26]. The mass ratio between nanomaterial and [BMIM][PF$_6$] was optimized, and further, nanocomposite gel was prepared by mixing 2 mg of SWCNT with 40 μL [BMIM][PF$_6$] ionic liquid. This ratio assured a 5% of nanomaterial loading, in order to decrease the background signal, being in concordance with data presented by Kachoosangi et al. [27]. This mixture was sonicated for 60 min until homogenous gel was obtained. A volume of 4 μL gel was added onto the screen-printed working electrodes and the resulted modified sensors were stored at room temperature.

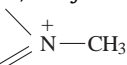### 2.4. Preparation of HRP-nanocomposite modified biosensors

For the preparation of the biosensors, the enzyme HRP was entrapped in SWCNT–[BMIM][PF$_6$] through a sol–gel matrix. Thus, 1 mg of HRP enzyme was dispersed in 50 μL [BMIM][PF$_6$] thoroughly, followed by addition of 2.5 mg SWCNTs and mixed together. Further, this composition was mixed with sol–gel in a ratio of 50:50 (vol.%) and a volume of 5 μL (5 IU HRP) was deposed onto the screen-printed working electrodes. The sol–gel matrix was prepared by hydrolysis of two alkoxide precursors: tetramethoxysilane (TMOS) and methyltrimethoxysilane (MTMOS) in a 5:15 ratio, and the hydrolysis time of the *sol* was about 6 h, according to the previous optimized procedures described by Gurban et al.

[28]. The obtained HRP–SWCNT–[BMIM][PF$_6$]/SPE biosensors were stored at 4 °C, in dry state.

3. Results and discussion

3.1. Characterization of SWCNT–[BMIM][PF$_6$] gel by Raman and FTIR spectroscopy

Raman spectrum of ionic liquid [BMIM][PF$_6$] is shown in Fig. 2A, curve a$_1$. The main Raman lines of [BMIM][PF$_6$] are situated at ca. 603–622, 742, 825, 1025, 1116, 1340, 1421, 1450, 1569, 2879, 2943, 2970 and 3170 cm^{-1}, they being associated with the following vibrational modes: $\diagup N^+ {-} CH_3$ symmetric stretching + ring out of plane deformation + CH$_2$ rocking + >N–CH$_2$–CH$_2$ bending, PF$_6^-$ stretching, CH$_2$ non-connected scissoring, ring deformation, C–C stretching, C–H ring in plane bending + CH$_2$ deformation, CH$_2$ wagging, ring asymmetric stretching + twisting of CH$_2$ group + CH$_3$ deformation, CH$_2$ bending, symmetric methyl stretches, Fermi resonance, anti-symmetric methyl stretches and symmetric C–H ring stretching, respectively [29,30].

Curves a$_2$ and a$_3$ of Fig. 2A show the Raman spectra of SWCNT before and after mixing with [BMIM][PF$_6$]. The spectrum of SWCNT exhibits the well-known three main groups of bands, whose relative intensity and peak position vary with excitation wavelength. In the first group, situated in the low frequencies range, 100–350 cm^{-1}, one finds the bands associated with radial breathing vibration modes (RBM) [31]. Accounting that the peak position of these bands are related to the tube diameter (d) through the relation ν (cm^{-1}) = 223.75/d (nm), the maxima at 179, 266, 314 and 331 cm^{-1} indicate tubes of different diameter of 1.25, 0.84, 071 and 0.67 nm, respectively. The second group, consisting of G and D bands, covers the interval from 1000 to 1700 cm^{-1}. These bands are not only related to the nanotube structure; G band peaking at about 1587 cm^{-1} is attributed to the tangential vibration mode it being observed in all graphitic materials. The D band, whose peak position varies with the excitation wavelength, is frequently associated with a disorder or defects state induced in the graphitic lattice or nanotubes [31]. The third group, located in the high wavenumbers range from 1700 to 3500 cm^{-1}, corresponds to the second order
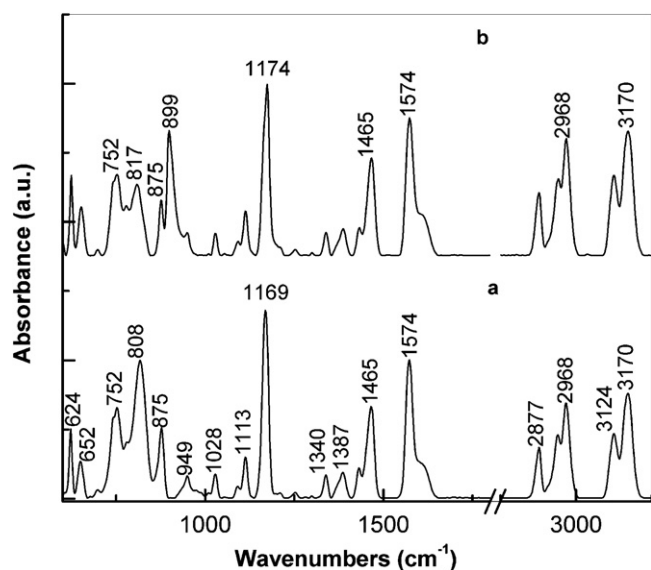
Fig. 3. FTIR spectra of [BMIM][PF$_6$] (a) and the SWNT-[BMIM][PF$_6$] gel (b).

Fig. 4. Cyclic voltammograms recorded at SPE (a), SWCNT/SPE (b) and SWCNT–[BMIM][PF$_6$]/SPE (c) electrodes (2 mM H$_2$O$_2$, scan rate 0.1 V s^{-1}).

Raman spectrum. The most intense band is detected at approximately twice the wavenumber of the D band.

Fig. 2A, curve a$_3$, reveals as main changes induced in the Raman spectrum of SWCNT–[BMIM][PF$_6$] gel: (i) an down-shift of the RBM band with maximum at 179 to 175 cm^{-1} and (ii) an increase in the intensity of the D band accompanied of an up-shift from 1282 to 1287 cm^{-1}. According to the theory, the two strongest bands observed in Fig. 2B at 196 and 380 cm^{-1} (solid curve), indicate that at 676 nm excitation wavelength the resonance occurs over a narrow range of diameters of tubes around 1.14 and 0.8 nm, respectively. Similar variations of the Raman spectra are observed at 676 nm excitation wavelength (Fig. 2B), for SWCNT–[BMIM][PF$_6$] gel as follows: (i) a down-shift of the RBM band with maximum at 196 to 189 cm^{-1}, (ii) an increase in the intensity of the D band accompanied with an up-shift from 1316 to 1321 cm^{-1} and (iii) a narrowing of the G band, change often correlated with an isolation process of tubes as result of the adsorption of molecules on the well side of tubes [32]. All these variations plead for an interaction between SWCNTs and IL, which can take place via the imidazolium ion through π–π or/and π–cationic interactions. Fig. 3 confirms the existence of such interaction.

The main absorption IR bands of [BMIM][PF$_6$] are localized at ca. 624, 652, 752, 808, 875, 949, 1028, 1113, 1169, 1340, 1387, 1465, 1574, 2877–2968, 3124 and 3170 cm^{-1}, these being attributed to the following vibrational modes: symmetric C–H out of plane bending + CH$_2$ rocking + >N–CH$_2$–CH$_2$ bending, C–N–C bending, C–H out-of plane bending of imidazole ring (–CH=CH–N), C–H out-of plane bending of imidazole ring (N–CH=N), C–H out-of plane bending of imidazole ring (=CH–N–CH=), CH$_2$ rocking, H–C–N bending, imidazole ring deformation, H–C–C stretching, symmetric C–H in plane bending + CH$_2$ deformation, ring breathing, CH$_3$ bending vibration, imidazole ring stretching, symmetric methyl C–H stretching, anti-symmetric and symmetric imidazolium C–H stretching vibration, respectively with three hydrogen atoms bound to the imidazolium ring [30]. In comparison with FTIR spectrum of [BMIM][PF$_6$], the following changes are remarked in the FTIR spectrum of SWCNT–[BMIM][PF$_6$] gel: (i) in the spectral range 700–830 cm^{-1} is observed an up-shift of the absorption band from 808 to 817 cm^{-1}, associated to the vibrational mode C–H out-of plane bending of imidazole ring (N–CH=N), which is accompanied of a change in the relative intensity of the two absorption bands with maximum at 752 and 808–817 cm^{-1} from 1:2 to 1:1,
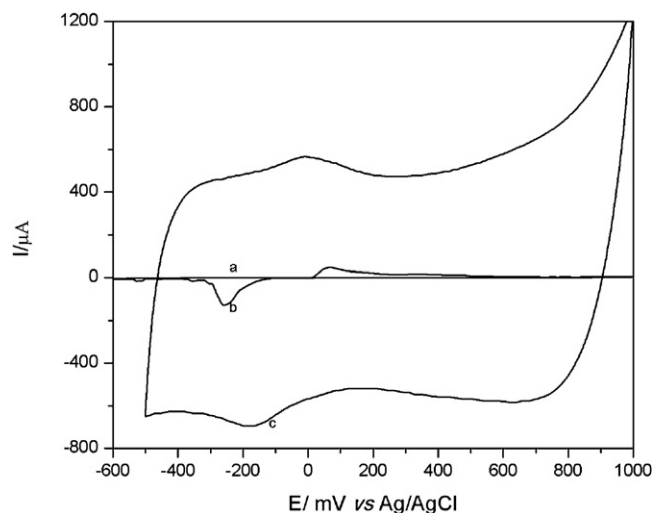
(ii) and up-shift of the absorption band associated to the vibration mode H–C–C stretching from 1169 to 1174 cm^{-1} and (iii) the appearance of a new band with maximum at 899 cm^{-1}. According to Kim et al. [33], the absorption band with maximum at 899 cm^{-1} does not belong to FTIR spectrum of SWCNTs, therefore this can be considered as an evidence of the interaction of SWCNTs with [BMIM][PF$_6$].

### 3.2. Voltammetric behaviour of the SWCNT–[BMIM][PF$_6$] modified electrodes

The electrocatalytic activity of the nanomaterial gel deposed onto the screen-printed carbon paste electrodes toward H$_2$O$_2$ reduction have been studied by voltammetry studies. The cyclic voltammetry experiments performed with modified screen-printed electrodes have demonstrated that nanocomposite film was formed onto the surface of carbon paste screen-printed electrodes. The recorded voltammograms for a 2 mM H$_2$O$_2$ solution in PBS, at unmodified and respectively, modified screen-printed electrodes are presented in Fig. 4.

One can observe that the peak of reduction current for SWCNT–[BMIM][PF$_6$] electrode is significant increased comparative with those obtained for SWCNT modified electrode, proving that SWCNT–[BMIM][PF$_6$] accelerate the electron transfer due to the presence of an electro-conductive network and a large active surface provided by SWCNT. The cathodic peak potential (E_{pc}) for SWCNT–[BMIM][PF$_6$] modified electrode was −0.188 V, assuring a considerable decreasing of the H$_2$O$_2$ overpotential. Wang et al. obtained a cathodic peak current at about −0.3 V using a platinum modified electrode with polyaniline-SWCNT–[BMIM][PF$_6$] composite, for H$_2$O$_2$ reduction [24].

The electrocatalytic activity of SWCNT–[BMIM][PF$_6$] toward H$_2$O$_2$ reduction has been studied by increasing the H$_2$O$_2$ concentration. One can observed a significant increase of the reduction peak current, showing the electrocatalytic activity of the SWCNT–[BMIM][PF$_6$] nanocomposite. A linear dependence of the cathodic peak currents with the H$_2$O$_2$ concentration was observed, being described by the linear regression: I (μA) = −9.7 [H$_2$O$_2$] (mM) − 107.98, with a correlation coefficient of 0.9963.

Using a simple method for modification of the screen-printed electrodes, the electrocatalytic activity toward H$_2$O$_2$ reduction has been improved and the cathodic peak potential was considerable decreased. Also, the SWCNTs can be easily dispersed in the imidazolium-based ionic liquid, forming a stable gel, in which
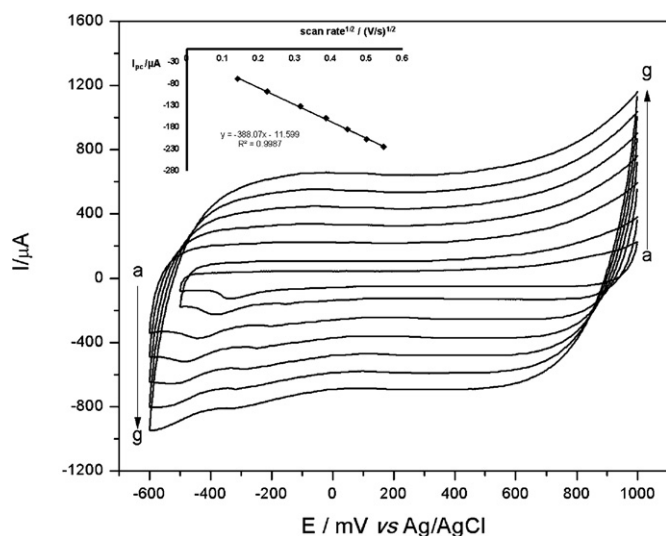
Fig. 5. Cyclic voltammograms of SWCNT–[BMIM][PF$_6$] modified screen-printed electrodes at scan rate: 0.02 (a), 0.05 (b), 0.1 (c), 0.15 (d), 0.2 (e), 0.25 (f) and respectively, 0.3 (g) V s^{-1}. Inset – plot of cathodic peak current (I_{pc}) vs. (scan rate)$^{1/2}$ (2 mM H$_2$O$_2$).

Fig. 6. EIS studies for SWCNT/SPE (a), SWCNT–[BMIM][PF$_6$]/SPE (b) and respectively HRP-SCWNT–[BMIM][PF$_6$]/SPE (c) in 5 mM Fe(CN)$_6$$^{3-/4-}$, containing 0.1 M KCl (frequency range 1 GHz–0.01 Hz, with a perturbation signal of 5 mV at open circuit potential). Inset – Randles circuit.

SWCNTs exists as network with much finer bundles, due to the cation–π interaction between imidazolium cations of IL and SWCNT surfaces [34]. Moreover, the mixing of SWCNT with [BMIM][PF$_6$] does not require any solvent and no disruption of the π-conjugated nanotube structure occurs [26]. On the contrary, Wang et al. [24] have used the electropolymerization of aniline in a SWCNT–IL matrix to improve the electrocatalytic activity toward H$_2$O$_2$ reduction, while Li et al. [25] enhanced the electrocatalytic activity toward H$_2$O$_2$ by the use of Prussian blue redox mediator electro-polymerized on carbon paste-[BMIM][PF$_6$] electrode.
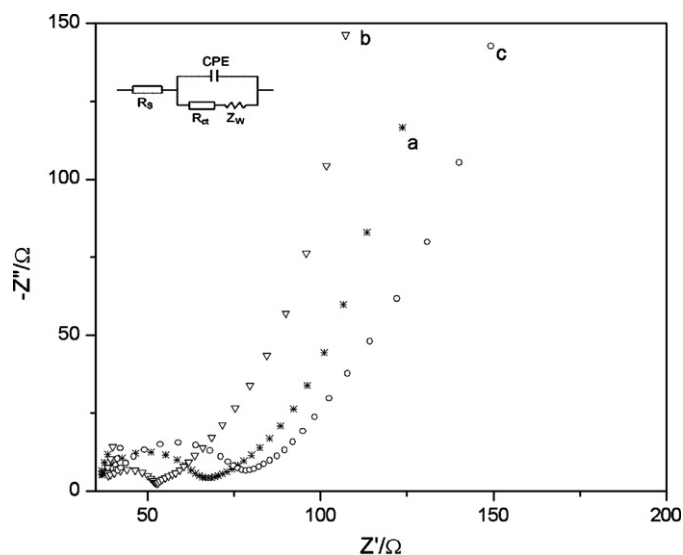
The effect of the scan rate on the SWCNT–[BMIM][PF$_6$] modified electrode responses for H$_2$O$_2$ 2 mM is shown in Fig. 5.

It can be observed that the reduction peak currents increase with the increase of the scan rate. Moreover, the reduction peak currents rise linearly with the square root of the scan rate (inset Fig. 5), suggesting that the reaction is controlled by diffusion process. A linear correlation between current peaks and scan rate usually shows that an electroactive substance is adsorbed on the electrode surface, thus means that the electron transfer between H$_2$O$_2$ and SWCNT–[BMIM][PF$_6$] was surface-controlled electrochemical process [35].

3.3. Amperometric behaviour of the SWCNT–[BMIM][PF$_6$] modified electrodes

Electrocatalytic activity of the modified screen-printed electrodes toward H$_2$O$_2$ reduction has been studied by amperometry. An optimisation of the working potential was done by carrying out measurements at different applied potentials vs. Ag/AgCl, using 0.2 mM H$_2$O$_2$ and taking into consideration the cyclic voltammetry studies performed above. Thus, a −0.2 V has been chosen to be the working potential for further amperometric studies. Calibration of the SWCNT–[BMIM][PF$_6$]/SPE and SWCNT/SPE were performed by successive additions of H$_2$O$_2$ 20 mM in PBS, reproducibility being determined by calibration of 3 sensors from different lots of electrodes, in the same experimental conditions. The specific sensitivity of the SWCNT–[BMIM][PF$_6$] modified sensors was about 64.3 ± 2.6 mA M^{-1} cm^{-2} (RSD = 4%) and the H$_2$O$_2$ was detected in a linear range from 0.02 to 2 mM, with a limit of detection by 11.2 μM.

The operational stability was evaluated by measuring the analytic responses of the modified sensors for 0.2 mM H$_2$O$_2$, at

an applied potential of −0.2 V. A good stability was obtained for SWCNT–[BMIM][PF$_6$] modified screen-printed electrodes, the average current for 20 repetitive measurements being 2.6 ± 0.1 μA, with RSD = 3.8%, while for SWCNT/SPE the average current was 1.6 ± 0.08 μA, with RSD = 5.1%.

In the absence of ionic liquid (see the SWCNT/SPE modified sensors) the detection performance was very poor. Thus the sensitivity was two times lower, the linear range was limited to one decade of concentration and the reproducibility was 6 times lower. Also, the response time was much longer (32 s) compared with 10 s in the case of composite gel modified sensors.

Based on these performances (high sensibility, faster response, better reproducibility and stability) it is envisageable that SWCNT–[BMIM][PF$_6$]/SPE could provide a highly sensitive analytical tool for the detection of estrogenic compounds.

Interferences studies were carried out using SWCNT–[BMIM][PF$_6$] based sensors, in the presence of some potentially interferences compounds, such as ascorbic acid, uric acid and acetaminophen. The tests were performed in 0.05 M phosphate buffer solution (pH 7.4), at working potential of −0.2 V vs. Ag/AgCl, by comparing the analytical responses obtained after addition of 0.2 mM H$_2$O$_2$ and 0.4 mM interfering compounds, respectively. A response of 2.6 μA was observed when H$_2$O$_2$ was added, while no considerable variations of the analytical signal were determined after additions of 0.4 mM ascorbic acid (0.1 μA), uric acid (0.03 μA) or acetaminophen (0.06 μA). All these results prove that, working at −0.2 V, the interfering effect of the studied compounds is negligible.

The voltammetric and amperometric studies carried out with SWCNT–[BMIM][PF$_6$]/SPE have shown that nanocomposite gel possess high electrocatalytic activity toward H$_2$O$_2$ reduction, accelerating the electron transfer between H$_2$O$_2$ and electrode.

For further experiments this nanocomposite will be used in order to prepare the bio-functional material for development of amperometric biosensors for endocrine disrupters detection.

3.4. EIS of the nanocomposite modified electrodes

The nanocomposite modified electrodes were studied by electrochemical impedance spectroscopy. The obtained impedance profiles exhibit a well-defined semicircle portion at higher

Table 1
Analytical parameters of HRP-SWCNT–[BMIM][PF$_6$] based biosensors ($n = 3$ electrodes).

Analyte	Specific sensitivity (mA M^{-1} cm^{-2})	RSD (%)	Linear range (μM)	LOD[a] (μM)	Response time (s)
Phenol	134 ± 9	6.6	6.2–282	2.8	26
4-t-Octylphenol	662 ± 2	1.8	5.5–97.7	1.1	5
4-n-Nonylphenol	296 ± 17	5.7	5.5–140	0.4	8

[a] (S/N = 3).

frequencies, with diameter equal to the electron transfer resistance (R_{et}), corresponding to the electron transfer process and a linear part at lower frequencies corresponding to the diffusion limited process. This resistance controls the electron transfer kinetics of the redox couple at the electrode interface, indicating that [BMIM][PF$_6$] can reduce R_{et}. Its value varies when different species are adsorbed onto the electrode surface, therefore this R_{et} is used to describe the interface properties of the electrode [17]. To fit the results, a simple equivalent Randles circuit has been used.

Fig. 6 presents the Nyquist profiles obtained for SWCNT, SWCNT–[BMIM][PF$_6$], and respectively HRP-SWCNT–[BMIM][PF$_6$] modified electrodes in 5 mM Fe(CN)$_6$$^{3-/4-}$ containing 0.1 M KCl. The R_{et} for SWCNT/SPE was found to be 30.2 Ω, while for SWCNT–[BMIM][PF$_6$]/SPE was 17.4 Ω. It can be seen that the addition of ionic liquid to carbon nanotubes facilitate the direct electron transfer, and this can be attributed to its excellent conductivity. When HRP was introduced in the nanocomposite structure by sol–gel entrapment, the value of the electron transfer resistance increased at 39.3 Ω. This might be due to the sol–gel matrix on the surface of the nanocomposite, functioning as barrier that made more difficult the interfacial charge transfer, or it might be caused by the macromolecular structure of HRP which blocks the redox species Fe(CN)$_6$$^{3-/4-}$. These results prove that the electron transfer is favoured by the presence of the nanocomposite gel based on SWCNT and [BMIM][PF$_6$] ionic liquid, due to the electrostatic interaction between positively charged electrode surface and negatively charged redox species Fe(CN)$_6$$^{3-/4-}$.

3.5. Optimisation and characterization of HRP-SWCNT–[BMIM][PF$_6$] based biosensors

The amperometric measurements with biosensors based on HRP-SWCNT–[BMIM][PF$_6$] nanocomposite were performed in a first attempt using phenol as electron donor substrate. After optimisation of analytical parameters and biosensors characterization using phenol as substrate, the 4-t-octylphenol and respectively 4-n-nonylphenol were determined.

3.5.1. Optimisation of the hydrogen peroxide concentration

At high concentration of hydrogen peroxide or in the presence of oxygen, an enzymatically inactive form of HRP (Compound III) can be formed [36,37], and the rapid inactivation of peroxidase during reaction course represents one of the main limitations of the sensitivity in peroxidase based assays. To avoid enzyme inactivation by excess of hydrogen peroxide and to achieve a good sensitivity, H$_2$O$_2$ concentration should be optimized.

The analytical responses of HRP-SWCNT–[BMIM][PF$_6$] biosensor were recorded for different concentrations of H$_2$O$_2$ ranging from 5 to 200 μM, using a phenol concentration of 50 μM and an applied potential of −0.2 V. An increase of the analytical responses for H$_2$O$_2$ concentration up to 60 μM was observed, followed by a continuous decrease of the responses for higher concentrations of H$_2$O$_2$. Hydrogen peroxide concentration of 60 μM was considered the optimal concentration and it was used for all further experiments.

3.5.2. Performance of HRP-SWCNT–[BMIM][PF$_6$] based biosensor for phenols detection

Phenol, 4-t-octylphenol and respectively 4-n-nonylphenol have been determined by calibration tests performed in the experimental conditions described above. The biosensor was characterized in terms of sensitivity, linear range, detection limit, response time and stability.

The analytical parameters obtained from the calibration curves and described by the linear regression are given in Table 1.

Biosensors based on HRP-SWCNT–[BMIM][PF$_6$] nanocomposite exhibited higher sensitivities and lower detection limits for the endocrine disrupters, 4-t-octylphenol and respectively, 4-n-nonylphenol, comparing with the biosensors based on HRP/SWCNT-Prussian blue modified screen-printed electrodes, developed in our previous work [16]. These results demonstrate a high catalytic activity of HRP, leading to an improvement of biosensor properties and enhancing the detection of endocrine disrupter chemicals, 4-t-octylphenol and respectively, 4-n-nonylphenol.

The planar characteristics of the sensors produced by screen-printed technique usually require a good and reproducible contact between transducer and enzymatic layer. The stability tests were performed by injection of 50 μM substrate (i.e. phenol, 4-t-octylphenol or 4-n-nonylphenol) in 0.05 M phosphate buffer containing 60 μM H$_2$O$_2$, at an applied potential of −0.2 V vs. Ag/AgCl.

Good stabilities were achieved with these biosensors, for 20 successive injections being obtained an average current of 1.48 $\pm$ 0.09 μA (RSD = 6.6%) for phenol, 1.12 $\pm$ 0.08 μA (RSD = 7.3%) for 4-t-octylphenol, and 1.14 $\pm$ 0.09 μA (RSD = 8.4%) for 4-n-nonylphenol, respectively.

4. Conclusions

The nanocomposite material, obtained by mixing SWCNTs with hydrophobic [BMIM][PF$_6$] ionic liquid has been used for the development of highly sensitive, stable and robust mediator-free biosensor, which was employed to detect some important metabolites, known as endocrine disrupters (i.e. 4-t-octylphenol and 4-n-nonylphenol). Formation of nanocomposite gel was evidenced in: (i) Raman spectra by an increase in intensity of the D band and an down-shift of the RBM band and (ii) FTIR spectra by the appearance of a new absorption band with maximum at 899 cm^{-1} and the changes of position of bands associated to the C–H out of plane bending and H–C–C stretching vibration modes. The CV and EIS studies highlight that SWCNT–[BMIM][PF$_6$] nanocomposite accelerate the electron transfer between hydrogen peroxide and electrode.

SWCNT–[BMIM][PF$_6$] gel was used as immobilising matrix to entrap horseradish peroxidase enzyme, providing a good microenvironment for enzyme, to retain its biocatalytic activity and to perform electrocatalysis of hydrogen peroxide, without using any mediator.

The HRP based biosensor ensured a detection of 4-t-octylphenol in a linear range from 5.5 to 97.7 μM, with a detection limit of about 1.1 μM, while 4-n-nonylphenol could be detected between 5.5 and 140 μM. The limit of detection for 4-n-nonylphenol was 0.4 μM (S/N = 3). Coupling the selectivity of the enzyme and

sensibility of the hydrogen peroxide sensor in a miniaturized system made possible to obtain a robust analytical device, which involve a good stability and reproducibility for detection of 4-t-octylphenol and respectively, 4-n-nonylphenol.

The obtained biosensors allowed a rapid detection of alkylphenols, offering the opportunity to be used further for detection of these endocrine disrupters in real samples.

Acknowledgement

References

[1] T. Colborn, M.J. Smolen, R. Rolland, Toxicology and Industrial Health 14 (1998) 14.
[2] T. Colborn, Environmental Toxicology and Chemistry 17 (1998) 2.
[3] I. Coille, S. Reder, S. Bucher, G. Gauglitz, Biomolecular Engineering 18 (2002) 273–280.
[4] P.T. Holland, Pure and Applied Chemistry 75 (2003) 1843–1857.
[5] P. Lopez-Roldan, M.J.L. de Alda, D. Barcelo, Analytical and Bioanalytical Chemistry 378 (2004) 599–609.
[6] E.E. Petrovic, M.J. Lopez de Alda, D. Barcelo, Trends in Analytical Chemistry 20 (2001) 637–648.
[7] J. Parellada, A. Narvaez, M.A. Lopez, E. Dominguez, J.J. Fernandez, V. Pavlov, I. Katakis, Analytica Chimica Acta 362 (1998) 47–57.
[8] Y.Z.H. Yin, S. Ai, Q. Chen, X. Zhu, X. Liu, L. Zhu, Journal of Hazardous Materials 174 (2010) 236–243.
[9] G.A. Evtugyn a, S.A. Eremin b, R.P. Shaljamova, A.R. Ismagilova, H.C. Budnikov, Biosensors and Bioelectronics 22 (2006) 56–62.
[10] M.K. Usami, Y. Ohno, Journal of Steroid Biochemistry and Molecular Biology 81 (2002) 47–55.
[11] Z.J. Yakovleva, J.Z. Zeravik, I.V. Michura, A.A. Formanovsky, M. Franek, S.A. Eremin, International Journal of Environmental Analytical Chemistry 83 (2003) 597–607.
[12] J.V. Samsonova, Maya Yu. Rubtsova, M. Franek, Analytical and Bioanalytical Chemistry 375 (2003) 1017–1019.
[13] D.D.E. Dempsey, A. Collier, Biosensors and Bioelectronics 20 (2004) 367–377.
[14] D.D.T.M. Portaccio, F. Arduini, M. Lepore, D.G. Mita, N. Diano, L. Mita, D. Moscone, Biosensors and Bioelectronics 25 (2010) 2003–2008.
[15] M.R. Montereali, L. Della Seta, W. Vastarella, R. Pilloton, Journal of Molecular Catalysis B: Enzymatic 64 (2010) 189–194.
[16] A. Arvinte, L. Rotariu, C. Bala, A.M. Gurban, Bioelectrochemistry 76 (2009) 107–114.
[17] J.L. Huang, Y.C. Tsai, Sensors and Actuators B: Chemical 140 (2009) 267–272.
[18] G.L. Ruzgas, J. Emneus, G. Marko-Varga, Journal of Electroanalytical Chemistry 391 (1995) 41–49.
[19] D.L. Compton, J.A. Laszlo, Journal of Electroanalytical Chemistry 520 (2002) 71–78.
[20] B.K. Sweeny, D.G. Peters, Electrochemistry Communications 3 (2001) 712–715.
[21] H.J. Chen, Y.L. Wang, Y. Liu, Y.Z. Wang, L. Qi, S.J. Dong, Electrochemistry Communications 9 (2007) 469–474.
[22] S.J.-Y. Fan, Huang Ke-Jing, Colloids and Surfaces B: Biointerfaces 76 (2010) 44–49.
[23] Z.X. Xu, T. Wan, C. Zhang, Microchimica Acta 172 (2011) 199–205.
[24] Q. Wang, Y. Yun, J. Zheng, Microchimica Acta 167 (2009) 153–157.
[25] X.L.Y. Li, X. Zeng, Y. Liu, X. Liu, W. Wei, S. Luo, Microchimica Acta 165 (2009) 393–398.
[26] T. Fukushima, A. Kosaka, Y. Ishimura, T. Yamamoto, T. Takigawa, N. Ishii, T. Aida, Science 300 (2003) 2072–2074.
[27] R.T.I. Kachoosangi, I. Abu-Yousef, J.M. Yousef, S.M. Kanan, L. Xiao, S.G. Davies, A. Russell, R.G. Compton, Analytical Chemistry 81 (2009) 435–442.
[28] A.-M. Gurban, T. Noguer, C. Bala, L. Rotariu, Sensors and Actuators B: Chemical 128 (2008) 536–544.
[29] C. Romero, T.R. Lee, S. Baldelli, J. Phys. Chem. C (2007) 240–247.
[30] R.W. Berg, Monatshefte für Chemie 138 (2007) 1045–1075.
[31] R. Saito, G. Dresselhaus, M.S., Dresselhaus, Imperial College Press, London, 1998, 35-70.
[32] M. Baibarac, M. Husanu, I. Baltog, Physica E: Low-dimensional Systems and Nanostructures 41 (2008) 66–69.
[33] U.J. Kim, X.M. Liu, C.A. Furtado, G. Chen, R. Saito, J. Jiang, M.S. Dresselhaus, P.C. Eklund, Physical Review Letters 95 (2005) 157402-1-4.
[34] D. Wei, A. Ivaska, Analytica Chimica Acta 607 (2008) 126–135.
[35] S.F. Wang, T. Chen, Z.L. Zhang, X.C. Shen, Z.X. Lu, D.W. Pang, K.Y. Wong, Langmuir 21 (2005) 9260–9266.
[36] J. Everse, K.E. Everse, M.B. Grisham, CRC Press, Boca Raton, Florida, Vol II (1991), 51-84.
[37] M. Gajhede, Horseradish Peroxidase , John Wiley & Sons, Ltd., 2006.